Structure, Vol. 11, 915–926, August, 2003, ©2003 Elsevier Science Ltd. All rights reserved. DOI 10.1016/S0969-2126(03)00149-7

Structure and Texture of Fibrous Crystals Formed by Alzheimer's Aβ(11–25) Peptide Fragment

Pawel Sikorski,[1,3] Edward D.T. Atkins,[1,*] and Louise C. Serpell[2]

[1] Physics Department
University of Bristol
Tyndall Avenue
Bristol BS8 1TL
United Kingdom

[2] Structural Medicine Unit
Department of Haematology
Cambridge Institute for Medical Research
Wellcome Trust/MRC Building
University of Cambridge
Hills Road
Cambridge CB2 2XY
United Kingdom

Summary

Amyloid fibril deposition is central to the pathology of Alzheimer's disease. X-ray diffraction from amyloid fibrils formed from full-length Aβ(1–40) and from a shorter fragment, Aβ(11–25), have revealed cross-β diffraction fingerprints. Magnetic alignment of Aβ(11–25) amyloid fibrils gave a distinctive X-ray diffraction texture, allowing interpretation of the diffraction data and a model of the arrangement of the peptides within the amyloid fiber specimen to be constructed. An intriguing feature of the structure of fibrillar Aβ(11–25) is that the β sheets, of width 5.2 nm, stack by slipping relative to each other by the length of two amino acid units (0.70 nm) to form β ribbons 4.42 nm in thickness. Aβ(1–40) amyloid fibrils likely consist of once-folded hairpins, consistent with the size of the fibers obtained using electron microscopy and X-ray diffraction.

Introduction

Amyloidoses are a group of degenerative diseases in which normally soluble proteins undergo a conformational change accompanied by aggregation and are deposited as amyloid fibrils in the tissues. Many different proteins have been identified that form amyloid in disease (Sunde and Blake, 1998); each is characterized by the protein comprising the amyloid fibrils. In the case of Alzheimer's disease amyloid, two closely related polypeptides consisting of 40 and 42 amino acids and known as Aβ comprise the fibrillar amyloid. These polypeptides are cleaved from a larger, transmembrane protein known as the amyloid precursor protein (APP; Selkoe, 1991).

Amyloid fibrils exhibit certain distinctive features. For example, Congo red staining reveals an apple green birefringence color under crosspolarized light, suggesting that amyloid fibrils are composed of a repeating structure capable of organizing the Congo red dye molecules along the length of the fibrils. Indeed, historically, amyloid was identified by staining with specific dyes (Virchow, 1854; Puchtler et al., 1961; Naiki et al., 1989). Transmission electron microscopy (TEM) and other nanoscale imaging techniques, such as atomic force microscopy (AFM), show amyloid to be long (μm range) fibrous entities, with lateral dimensions in the range of 7–10 nm. In addition, the fibrils can display fibrillation, (axial) twisting, and ribbon-like characteristics. However, to date, the most crucial identifying feature of amyloid is the nature of the X-ray (or electron) diffraction data. Amyloid fibrils display a distinctive X-ray diffraction fingerprint (Eanes and Glenner, 1968; Sunde et al., 1997) that emanates from the "cross-β" structure (Rudall, 1946, 1950, 1952), one of the small number of explicit and repetitive protein conformations. The first detailed structural model for the cross-β conformation in proteins was described by Geddes and coworkers in 1968 (Geddes et al., 1968). More recently, other versions have been described (Krejchi et al., 1997). In the cross-β structure, the protein chains run orthogonal to the fibril direction and are hydrogen bonded (interchain spacing 0.47 nm) in an orchestrated manner to form a β sheet (Geddes et al., 1968; Krejchi et al., 1997; Pauling and Corey, 1953), as illustrated in Figure 1. A crystallographic repeat of 0.70 nm is evident along the pleated β chain (i.e., with an axial advance per peptide unit of 0.35 nm and arranged with a 2-fold helical repeat). The spacing between the β sheets is variable and depends on the size of side chain groups, from 0.37 nm for polyglycine (Fraser and MacRae, 1973) to 1.40 nm for calcium salts of polyglutamic acid (Keith et al., 1969). The peptide chains may be arranged in an antiparallel (Figure 1A) or parallel (Figure 1B) fashion, or possibly a mixture (Serpell, 2000). The positions of the principal diffraction signals provide the key to unraveling the texture and basic crystallographic structure of the specimen.

Study of the structure of mature amyloid fibrils has been problematic due to the insoluble and heterogeneous nature of the fibrils. Ex vivo preparations can often be contaminated and the harsh extraction procedure can damage the structure. Amyloid fibrils can be assembled in vitro, allowing the study of pure protein amyloid fibrils. TEM studies reveal that amyloid fibrils from many different sources exhibit similar morphological features. X-ray diffraction has been used to examine the structure of Alzheimer's amyloid formed from full-length and fragments of Aβ (Inouye et al., 1993; Inouye and Kirschner, 1997; Malinchik et al., 1998).

In particular, Aβ(11–25) has been found to form ordered amyloid fibrils, exhibiting similar morphology to those of full-length Aβ (Serpell and Smith, 2000; Serpell et al., 2000). This peptide is located in a central region of Aβ, thought to be important in fibril formation (Serpell, 2000) and may represent the core structure of amyloid fibrils (Serpell et al., 2000). High-resolution cryo-electron microscopy was used to examine the molecular struc-

*Correspondence: e.atkins@bristol.ac.uk
[3] Present address: Department of Physics, Norwegian University of Science and Technology, Trondheim, Norway.

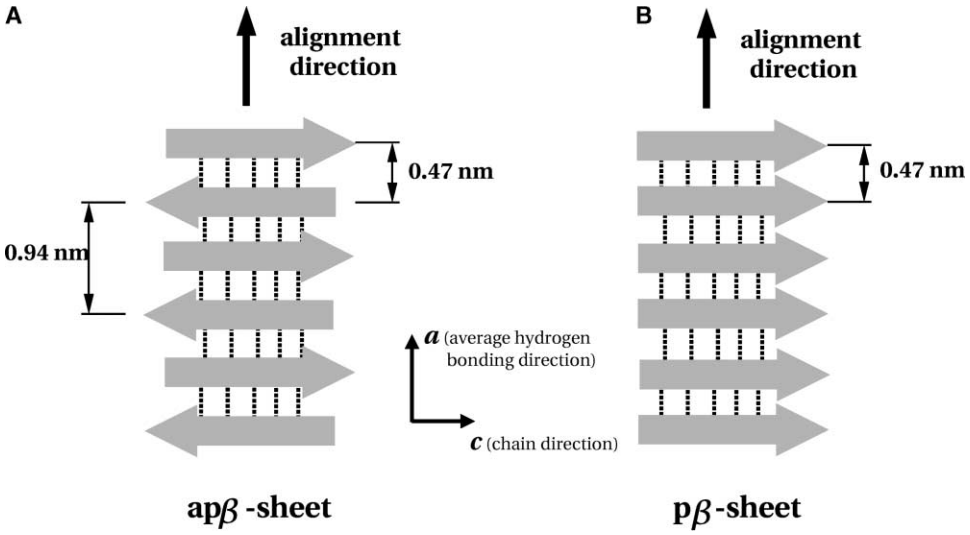

Figure 1. Views, Orthogonal to the Surface, of a Schematic Cross-β Hydrogen-Bonded Sheet

Chain segments and hydrogen bonds are represented by arrowed strips and dotted lines, respectively.
(A) Antiparallel β sheets; for a long protein chain, these antiparallel segments would be connected by reverse turns. The crystallographic repeat is twice the characteristic 0.47 nm intrasheet, interchain spacing.
(B) For shorter chains, the chain segments can be in parallel.

ture of amyloid fibrils composed of Aβ(11–25) embedded in ice (Serpell and Smith, 2000). Electron micrograph images of selected single fibrils showed a regular set of transverse striations across the whole fibril at a spacing of 0.47 nm, directly revealing the cross-β structure. Magnetic field alignment was used to orient Aβ(11–25) amyloid fibrils (Serpell et al., 2000) for X-ray diffraction, and two discrete orientations of the fibers were found, orthogonal and axial. This unusual feature revealed that the fibrous sample exhibited a preferred texture, because separate X-ray diffraction patterns obtained with the incident beam directed in three mutually orthogonal directions gave distinctly different patterns. The X-ray diffraction pattern obtained with the incident beam parallel to the fiber axis revealed discrete arcs rather than diffraction rings, ruling out cylindrical fiber symmetry. A model of fibrils composed of once-folded peptide hairpins, associating in paired duplexes, was suggested for Aβ(11–25) crystals grown in an applied magnetic field (Serpell et al., 2000). However, closer examination of these X-ray data, together with new information, has cast doubts on some aspects of this particular model and revealed that the peptide chains form extended, unfolded β strands.

Here, we reexamine the original X-ray diffraction patterns obtained from Aβ(11–25) crystallized in an applied 2 Tesla magnetic field in greater detail, and have been able to derive a new and detailed three-dimensional structure for this oligopeptide. The calculated diffraction pattern is tested against the experimental data to ensure that there is a convincing match. We also introduce some additional fiber X-ray diffraction data and TEM images obtained from Aβ(11–25) and compare these results to those obtained from the longer Aβ(1–40) amyloid fragment.

Results

Morphology of Aβ(1–40) and Aβ(11–25) Amyloid Fibrils

A TEM image obtained from self-assembled Aβ(11–25) peptide is shown in Figure 2A. Long (many μm), thin ribbon-like or fibrillar strands are seen with a strong suggestion of twisting, but without any obvious long-range periodicity. The ribbons are close to 5 nm in width. This value is commensurate with the calculated length of 5.2 nm for Aβ(11–25) in the β conformation. Figure 2B shows similar ribbon-like strands obtained from self-assembled Aβ(1–40) peptide molecules. If the molecules were in the unfolded β conformation, the widths would be expected to be 14 nm, that is, 270% wider than for the Aβ(11–25) peptide molecules. However, the maximum widths seen are only 7 nm. This would suggest that the Aβ(1–40) molecules are once-folded hairpins in this preparation or that some regions of the peptide are not involved in the core structure of the fiber.

Comparison of X-Ray Patterns from Amyloid Fibers of Aβ(11–25) and Aβ(1–40)

The X-ray diffraction patterns from drawn fibers of Aβ(11–25) and Aβ(1–40) amyloid are compared in Figures 2C and 2D. Both exhibit the basic cross-β diffraction fingerprint with the 0.47 nm diffraction signal on the meridian, and many of the essential features are the same, suggesting a similar molecular organization. The shorter Aβ(11–25) peptide fragment yields better quality and higher resolution X-ray diffraction data and therefore offers the opportunity to extract more detailed structural information than for the Aβ(1–40) amyloid fibrils.

The X-ray diffraction pattern of a fiber obtained from

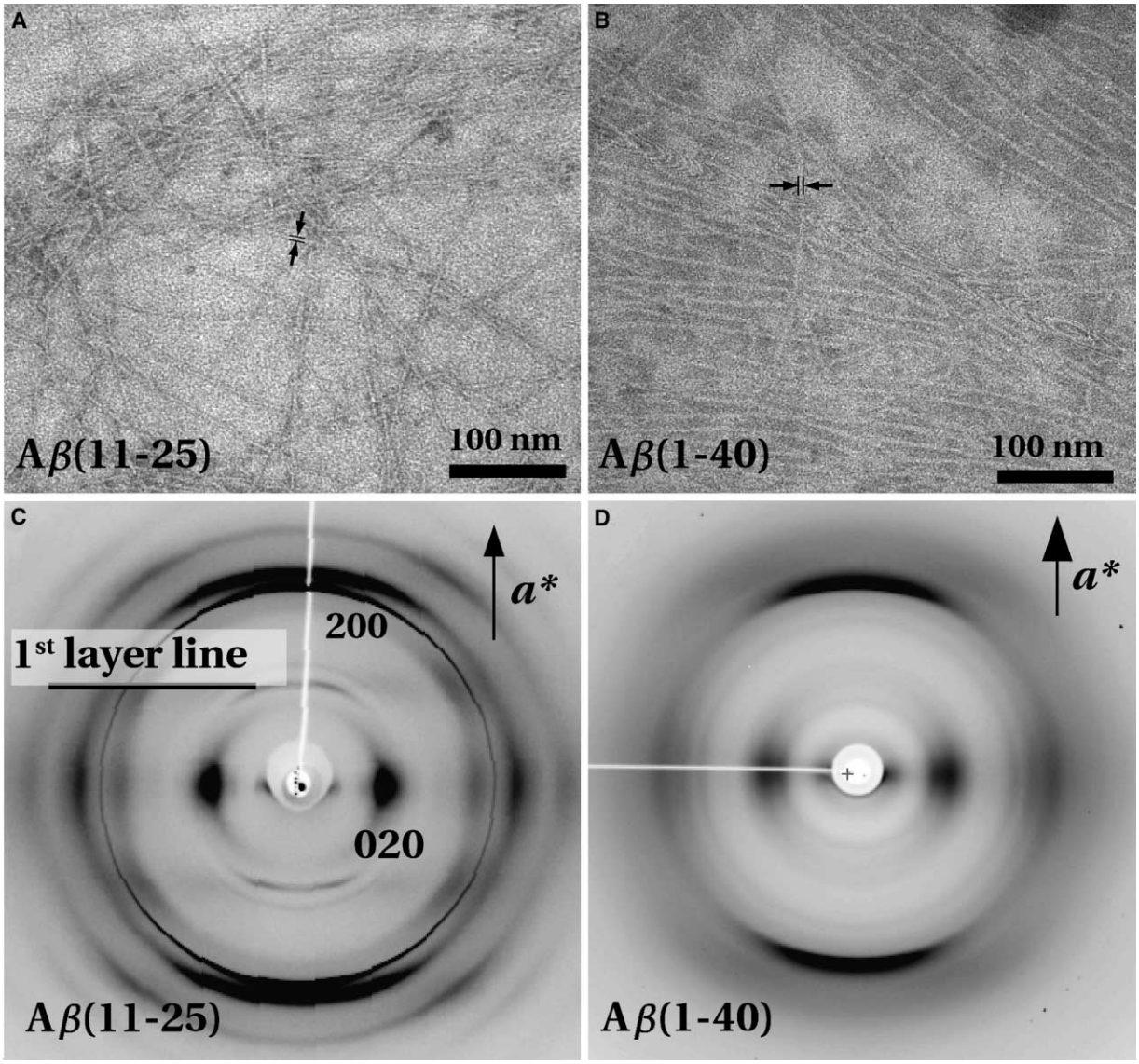

Figure 2. Electron Micrographs and Wide-Angle X-Ray Diffraction Patterns from Cross-β Ribbons of Self-Assembled Aβ Fragments

(A) Negatively stained electron micrograph of the Aβ(11–25) fragment; the measured width of ~5 nm (see arrowed markers) is commensurate with a nonfolded Aβ(11–25) peptide in the extended β conformation.

(B) The Aβ(1–40) fragment; the maximum estimated width is ~7 nm.

(C) Aβ(11–25) and (D) Aβ(1–40). Wide-angle X-ray patterns; fiber axis (*a**) vertical.

Aβ(11–25) is shown in Figure 2C. The pattern exhibits the characteristic cross-β fingerprint: a meridional arc at 0.47 nm (200) and a strong equatorial diffraction signal (020) at 1.06 nm. This latter value represents the intersheet stacking periodicity, controlled by the amino acid side groups, and falls within the range 0.37 nm (Fraser and MacRae, 1973) to 1.40 nm (Keith et al., 1969), as mentioned in the Introduction. The diffraction signals can be indexed on a monoclinic unit cell with parameters $a = 0.942$ nm; $b = 2.500$ nm; c (chain axis) $= 0.697$ nm; $\alpha = 122°$; $\beta = \gamma = 90°$. The details of the *d*-spacings and indexing, together with the reciprocal unit cell parameters, are given in Tables 1 and 2. There is noticeable first layer line (0.94 nm) diffraction consistent with an antiparallel β sheet structure (Geddes et al., 1968; Krejchi et al., 1997; Fraser and MacRae, 1973). The angular spread of the sharp 200 (0.47 nm) diffraction signal is noticeably greater than the other diffraction signals; indeed, a proportion of 200 diffraction poles occurs at all azimuths generating a diffraction ring. This suggests that some cross-β entities are not (fully) responding to the external orienting forces. A possible and plausible explanation of this feature is as follows. The first stage of the self-assembly and growth of the peptides is the formation of Aβ(11–25) cross-β ribbons. The strong, characteristic diffraction fingerprint of an individual ribbon is simply a sharp 0.47 nm diffraction signal representing the repetitive interchain distance between hy-

Table 1. Observed and Calculated *d*-Spacings and Indexing

			Fiber		Aligned in Magnetic Field		
			d_{obs} (nm)	d_{cal} (nm)	(a) d_{obs} (nm)	(b) d_{obs} (nm)	(c) d_{obs} (nm)
		SP_1	4.42	4.42	4.42		
		SP_2	2.21	2.21	2.21		
		SP_3	1.47	1.47	1.46		
h	*k*	*l*					
0	2	0	1.06	1.06	1.06	*	1.06
0	4	$\bar{1}$		0.57			0.60
0	4	0	0.53	0.53	0.53	0.52	0.53
0	2	1	0.43	0.43	0.43	0.42	0.43
0	6	$\bar{1}$		0.41	0.40		0.42
0	6	$\bar{1}$		0.41			
0	6	0		0.35			0.35
0	2	$\bar{2}$	0.35	0.35			
0	4	$\bar{2}$		0.35	0.35		0.36
0	6	$\bar{2}$	0.33	0.33		0.33	
0	8	$\bar{2}$		0.29	0.30		
0	2	2		0.25	0.25		
1	0	0	0.95	0.94		0.95	
1	1	0	0.87	0.86	0.86		
1	2	0	0.70	0.70	0.70	0.69	
1	0	1	0.51	0.50	0.52	0.50	
1	2	0	0.44	0.46			
1	4	0		0.46		0.48	
1	$\bar{4}$	2	0.27	0.27			
2	0	0	0.47	0.47	0.47	0.47	0.47
2	2	0	0.44	0.43	0.43	0.43	
2	2	$\bar{1}$		0.39		0.39	
2	0	1	0.37	0.37	0.37	0.37	
2	2	1	0.32	0.32	0.32	0.31	
3	2	0		0.30	0.31		
4	0	0	0.24	0.24	0.24	0.24	
4	2	0	0.23	0.23	0.23	0.23	
4	2	$\bar{1}$		0.22	0.22	0.22	
4	2	$\bar{1}$	0.22	0.22			
4	0	1	0.22	0.22	0.22	0.22	

(a), (b), and (c) correspond to X-ray patterns shown in Figures 3A, 3B, and 3C, respectively.
*The overlying tails of a number of different diffraction signals make identification and measurement difficult in the reciprocal space region in this particular X-ray pattern.

drogen-bonded peptides. Thus, if the stress field(s) and surface tension forces that occur on sample preparation (see Experimental Procedures) do not preferentially orient these more delicate individual cross-β ribbons, then the 200 diffraction poles will distribute themselves in an attenuating manner from the orientation direction (vertical axis in Figure 2C) at all azimuths. The X-ray diffraction pattern obtained from fibers of Aβ(1–40) is shown in Figure 2D for comparison. Importantly, the absence (or relative weakness) of the 0.94 nm layer line in the Aβ(1–40) diffraction pattern does not *necessarily* indicate a parallel arrangement of β sheets (see Figure 1B). In a structure consisting of stacked β sheets (indicated by appearance of 0k0 diffraction signals), the first (and successive odd order) layer line may be cancelled out. Examples of this are discussed by Krejchi et al. (1997) and Geddes et al. (1968). Indeed, as discussed above, the size of the Aβ(1–40) fibrils (≤7 nm), as measured from TEM images (Figure 2B), is inconsistent with extended β chains 40 amino acids long (≈14 nm).

Table 2. Real and Reciprocal Monoclinic Unit Cell Parameters

a	0.942 nm	*a**	1.062 nm^{-1}
b	2.500 nm	*b**	0.472 nm^{-1}
c	0.697 nm	*c**	1.692 nm^{-1}
α	122°	α*	58°
β	90°	β*	90°
γ	90°	γ*	90°

We have chosen *a* to be the unique axis to maintain convention with the classic cross-β structure although the usual convention is to choose *b* or *c* to be the unique axis in monoclinic systems.

Aβ(11–25) Sample Crystallized in a Magnetic Field

The size (∼1 mm) and shape of the sample composed of aligned Aβ(11–25) crystallites and prepared in a 2 Tesla magnetic field enabled X-ray diffraction patterns to be obtained with the incident beam directed along different directions relative to the direction of the magnetic field. Figures 3A–3C show the X-ray diffraction

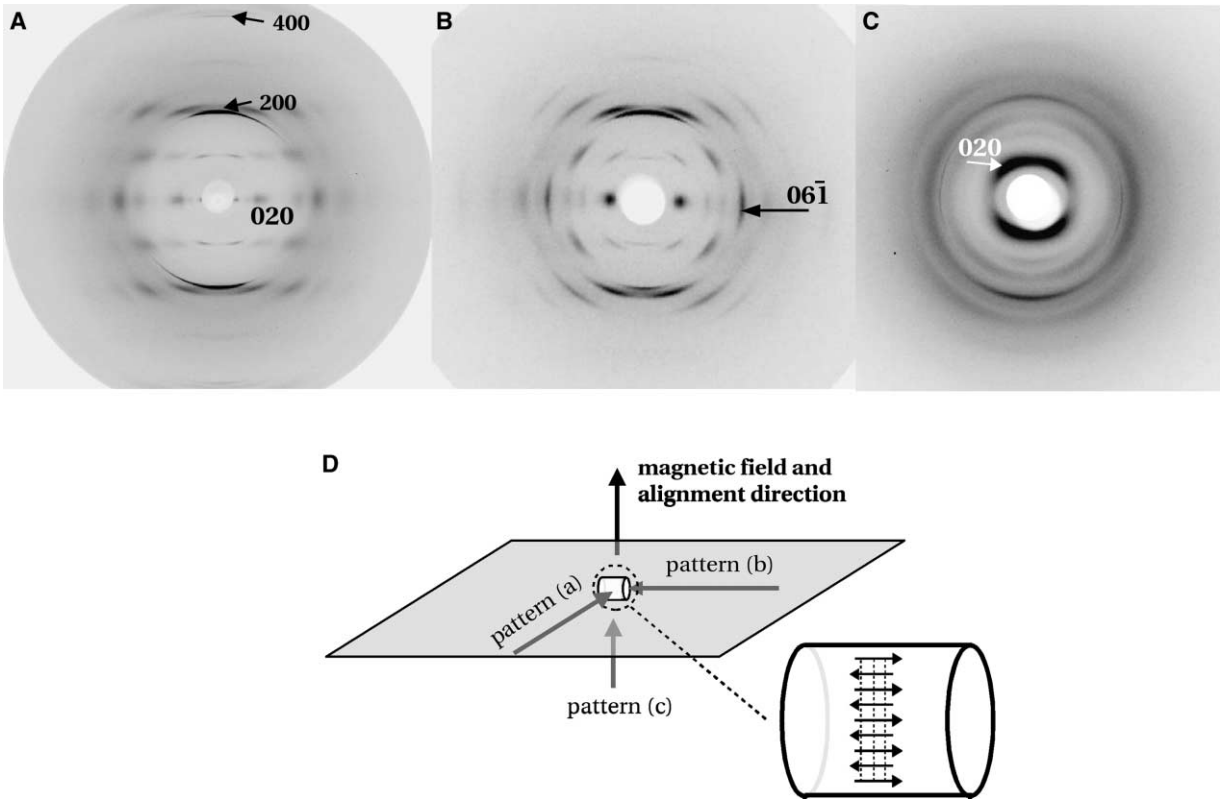

Figure 3. Wide-Angle X-Ray Diffraction Patterns Obtained from the Aβ(11–25) Oligopeptide Self-Assembled and Aligned in a Magnetic Field

Alignment direction vertical. In (A) and (B), the incident X-ray beam is orthogonal to the alignment direction and along the two directions indicated in (D), respectively. In (C), the incident X-ray beam is parallel to the alignment direction.

patterns obtained with the incident beam directed along the three mutually orthogonal axes relative to the cylindrically shaped sample, as illustrated in Figure 3D. The composite diffraction signals in all three diffraction patterns (Figures 3A–3C) of this Aβ(11–25) aligned in a magnetic field index on the *same* monoclinic unit cell as was deduced from the fiber diffraction pattern (Figure 2C). Thus, we believe that the crystal structure of Aβ(11–25) is the same in the sample that self-assembled and aligned in the magnetic field and that in the drawn fiber; what differs is the texture. A comparison of *d*-spacings and indexing is given in Table 1.

The X-ray diffraction patterns shown in Figures 3A and 3B are obtained with the incident beam orthogonal to the applied magnetic field direction and mutually orthogonal to each other (see Figure 3D). In both diffraction patterns, the observed Bragg diffraction signals are distributed on the layer lines at a spacing of 0.94 nm and with strong meridional diffraction signals appearing at 0.47 nm (200) and 0.236 nm (400); thus, the a^* axis is along the meridian. Consequently, the hydrogen bond direction (*a* axis) is aligned with the magnetic field direction. The *h*00, for odd *h*, appears to be systematically absent, consistent with the hydrogen-bonded β sheet arrangement shown in Figure 1A. The presence of the 0.94 nm layer line (100) suggests an antiparallel arrangement of hydrogen-bonded peptide chains (Geddes et al., 1968; Krejchi et al., 1997). The variation in the relative intensities of the diffraction signals observed in the patterns in Figures 3A and 3B are particularly noticeable on the equator (b^*c^*-reciprocal plane). This variation firmly suggests that the sample texture is different from that usually observed in straightforward fiber X-ray diffraction patterns. In the fiber texture, the crystallites are aligned with one crystallographic axis parallel to the alignment direction, and with random azimuthal dispersion (i.e., cylindrical symmetry) around the alignment axis. In this case, the azimuthal dispersion around the alignment axis is *not* random. The asymmetric nature of the arced tails of the exceptionally strong 200 diffraction signal, especially noticeable in Figure 3A, is similar to the feature we have already discussed in the fiber X-ray diffraction pattern (Figure 2C). The meridional *h*00 diffraction arcs are sharper (in the radius vector direction) than the equatorial 0*k*0 diffraction signals, even allowing for line broadening and other geometric correction factors. Thus, it would appear that the Aβ(11–25) amyloid 15-mer has self-assembled and grown in the hydrogen-bonding direction (*a* axis) to create a crystalline entity that has longer-range order in this *a*-direction relative to the directions perpendicular to the *a* axis. Worcester (1978) has discussed the structural origins of diamagnetic anisotropy in proteins and concluded that for β structures, the alignment of the hydrogen-bonding direction parallel to the direction of applied magnetic field is expected.

Figure 3C is the X-ray diffraction pattern obtained with the incident beam parallel to the magnetic field axis. The

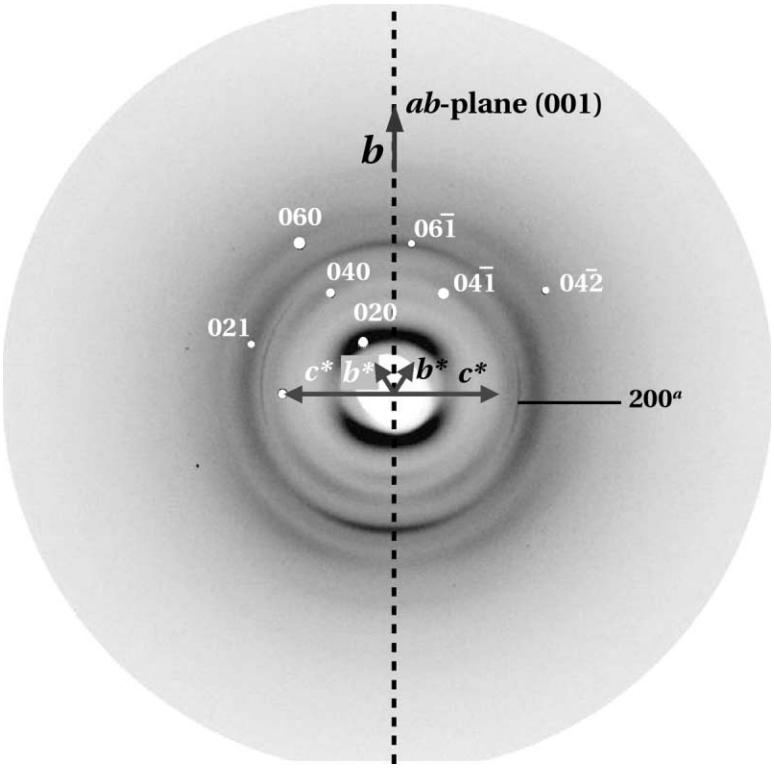

Figure 4. Enlarged Version of Figure 3C, Overlaid with the Calculated Positions of the *0kl* Diffraction Signals Based on the Monoclinic Unit Cell Given in Table 2

The diffraction signals belong to twins (black and white); only the white diffraction spots are indexed to avoid confusion. The composition *ab*-plane is shown by a dotted line. The angle *b**^*c** (turns out to be α*; see Tables 1 and 2) is measured to be 58°. 200[a]: this noticeably sharp d_{200} diffraction signal does not belong to the [100] crystallographic zone but comes from cross-β ribbons that are not aligned with their long *a* axis parallel to the orientation axis (see text).

presence of discrete pairs of X-ray diffraction signals confirms that the sample does not have cylindrical (fiber) symmetry. If the sample had fiber texture it would have given a series of concentric diffraction rings. Thus, in the magnetic field-aligned Aβ(11–25) crystal, a preferred crystalline texture exists (Alexander, 1969); indeed, the data suggest two distinct azimuthal orientations arranged symmetrically on either side of the vertical axis, a feature reminiscent of crystal twinning. A measure of the frequency of composition planes within the sample requires further investigation; there may only be a central composition plane.

This X-ray diffraction pattern (Figure 3C) represents the [100] zone axis, or 0*kl* reciprocal plane, and Figure 4 is an enlargement of this diffraction pattern with additional information overlaid to aid with the interpretation of the diffraction data. The X-ray pattern displays the *ab*-composition plane (001), and the *b**, *c** axes for each of the two twinned lattices are shown, marked in black and white, respectively. In order to reduce complexity, we will concentrate on just one (white) of the two twin-related lattices. The strongest diffraction signal, with a *d*-spacing of 1.06 nm and located at an angle of 58° (α*) from the horizontal axis, is the 020; the weaker fourth and sixth orders are also present (see Table 1). The 020 diffraction signal represents the intersheet stacking periodicity. There is a medium-intense and relatively sharp signal with the spacing of 0.43 nm (06$\bar{1}$) and a direction close to the *b* axis (inserted in Figure 4). This same diffraction signal is also evident in Figure 3B, where, of course, it falls on the equator, thus enabling us to geometrically link all three diffraction patterns (Figures 3A–3C) into a composite. A weak but sharp 200 diffraction signal also appears in Figures 4 (marked 200[a] in black) and 3C; this diffraction signal is forbidden in this [100] zone axis but occurs because not all cross-β ribbons are aligned, as explained above.

Small-angle X-ray diffraction patterns obtained from Aβ(11–25) aligned in a magnetic field and from the drawn fiber are shown in Figures 5A and 5B, respectively. Both X-ray diffraction patterns exhibit an equatorial diffraction signal at a spacing of 4.42 nm. In the X-ray diffraction pattern of a fiber taken at shorter specimen to film distance (Figure 6A), two progressively weaker equatorial diffraction peaks at 2.21 nm and 1.46 nm, respective second and third orders of 4.42 nm, are observed (see Table 1). This feature is common when lamellae or ribbons stack; they generate a one-dimensional lattice. In this case, the periodicity would represent the stacking periodicity of cross-β lamellae and be commensurate with the width of the cross-β ribbon. An estimate of the quality of the lattice can be made from the number of diffraction orders that occur; in this particular instance, the lattice dies away after the third order. That such a one-dimensional (super) lattice occurs is not a surprise, because we know a priori that the molecule is only 15 peptides long and so we would expect a diffraction signal(s) with spacing related to the length of the molecule. The Aβ(11–25) molecule in the β conformation is 5.2 nm long, and to foreshorten this value to match the experimental value of 4.42 nm we would need to project the molecules through an angle of $\cos^{-1}$(4.42 nm/5.2 nm) = 31.8°. In terms of a shear angle, this would be 31.8° + 90° = 121.8°. This value would appear to be directly related to the monoclinic unit cell angle $\alpha = 122°$ obtained when indexing the wide-angle X-ray diffraction data (see Tables 1 and 2), and to the angle between *b** and *c** measured to be 58° on the X-ray diffraction pat-

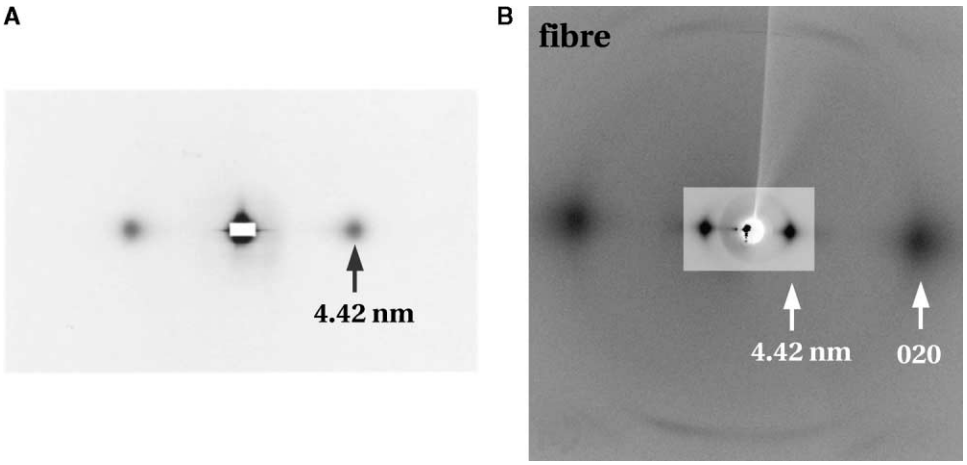

Figure 5. Small-Angle X-Ray Diffraction Patterns from the Aβ(11–25) Fragment, Taken with the Incident Beam Perpendicular to the Alignment Axis, Showing the 4.42 nm Equatorial X-Ray Diffraction Peak

Alignment and fiber axes are vertical.

Taken from the sample aligned in a 2 Tesla magnetic field (A) and from a fiber (B). The background level in the rectangular central region in (B) has been reduced in order to make the 4.42 nm diffraction peak clearer to see. The 4.42 nm spacing can be calibrated from the wide-angle diffraction signals that also appear; hence, we are confident of its value.

tern shown in Figure 4. In this diffraction pattern, the actual angle measured is the α^* angle, and for a monoclinic (*a* axis unique) unit cell, $\alpha = 180 - \alpha^* = 122°$.

Structure of Aβ(11–25)

The nonzero intensities of the diffraction signals on the first layer line (1*kl* at 0.942 nm) provide direct evidence that the hydrogen-bonded sheets are composed of molecules that hydrogen bond together in an antiparallel fashion. [We have no evidence that the peptide side chains in Aβ(11–25) crystals conspire to generate a precise, successively alternating spatial arrangement (with a repeat of 0.942 nm) in the *a*-direction in an otherwise parallel chain, hydrogen-bonded ribbon.] A model of the Aβ(11–25) cross-β sheet arrangement is shown in Figure 7A; the width of a single cross-β ribbon is 5.2 nm. Figure 7B shows a model where the cross-β ribbons stack directly onto each other in a common type of cross-β sheet stacking. The Aβ(11–25) cross-β ribbons are stacked 1.06 nm apart and there is *recuperative* intersheet slip (≈*a*/4; Geddes et al., 1968; Krejchi et al., 1997) in the *ac*-plane parallel to the *a* axis. Because of the pronounced crimping of the sheets, slippage can only reasonably occur parallel to the *c* axis in approximately integer multiples of the crimp repeat (structural *c*-repeat) of 0.697 nm. Figure 7C shows a structure similar to Figure 7B but there is an additional *progressive* slip of one whole crimp (structural *c*-repeat) of 0.697 nm in the *ac*-plane parallel to the *c* axis. Thus, the angle of shear is $(90° + \tan^{-1}[0.697\ \text{nm}/1.06\ \text{nm}]) = 123.3°$; this value is close (within 1.2%) to the monoclinic unit cell α angle (122°; see Table 2) obtained from the wide-angle X-ray data and the angle of 121.8° deduced from the low-angle X-ray diffraction data. Thus, we believe the long, self-assembled Aβ(11–25) cross-β ribbons to be approximately 5 nm wide. Seen as individual ribbons in Figure 2A, they stack with recuperative *a* axis interribbon shear (≈*a*/4 = 0.235 nm) and progressive *c* axis interribbon shear to generate nanotapes 4.42 nm in thickness as shown in Figure 8. These nanotapes also stack to form a one-dimensional lattice with a stacking periodicity of 4.42 nm. The quality of this lattice is able to sustain the fundamental and two orders. The calculated X-ray fiber diffraction (fiber axis is *a*) is shown in Figure 6B.

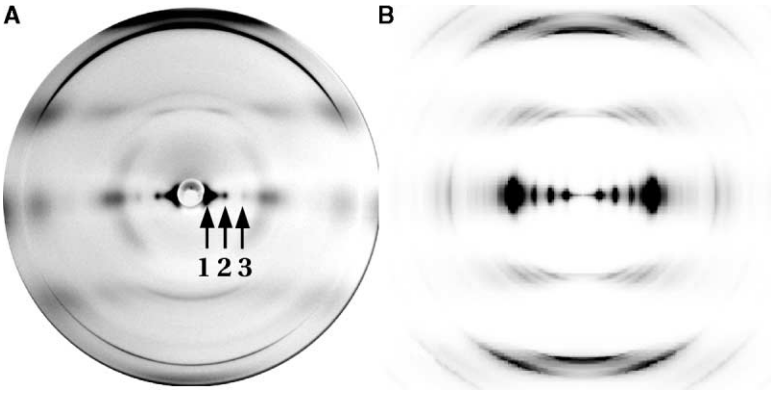

Figure 6. Comparison of Experimental and Calculated X-Ray Diffraction Data from Aβ(11–25) Fibers

(A) Wide-angle X-ray diffraction of a fiber with shorter specimen to film distance to that shown in Figure 5B in order to also show the 4.42 nm equatorial peak (marked 1) close to the beam stop, and with two progressively weaker orders (marked 2 and 3, respectively). These small-angle diffraction signals are referred to as SP_1, SP_2, and SP_3 in Table 1.

(B) Calculated X-ray fiber diffraction pattern from the proposed cross-β crystal structure of Aβ(11–25) (Tables 1 and 2; Figures 7C and 8).

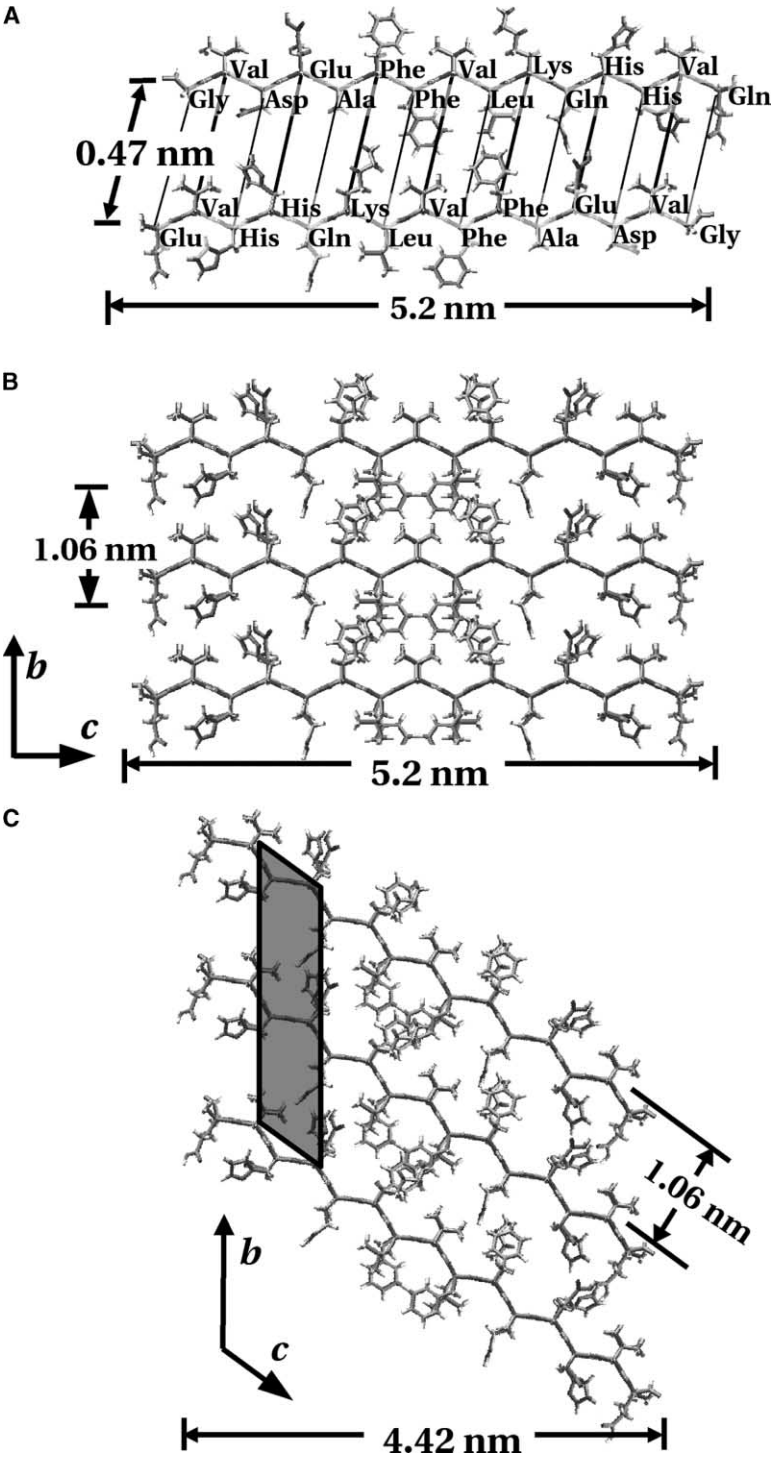

Figure 7. The Model of the 15-Mer Aβ(11–25)

(A) Oblique view of an antiparallel, two-chain pair of Aβ(11–25) molecules in the cross-β structure. The distribution of side groups on both surfaces can be seen. The 0.47 nm spacing (*a*-direction) is controlled by hydrogen bonding and the molecules are ~5 nm in length.

Stacking of Aβ(11–25) cross-β ribbons is 10.6 nm apart.

(B) Direct stacking that would generate an orthorhombic unit cell.

(C) Stacking with a slip of 0.697 nm (one β sheet crimp; one structural repeat in the *c*-direction) parallel to the *c* axis. This stacking arrangement gives rise to the monoclinic unit cell shown in the shaded box (see Table 2). In both cases, there is a recuperative *a* axis slip (~*a*/4) in the *ac*-plane.

In this case the stacking periodicity, and its second and third orders appear, and the pattern can be compared with the experimental X-ray diffraction pattern shown in Figure 6A. The overall match is good, suggesting that the basic ingredients of the proposed structure are correct.

Figures 9A and 9B compare the experimental and calculated wide-angle X-ray fiber diffraction patterns, respectively. In this case, the calculation is based of the monoclinic sublattice, and therefore the small-angle equatorial diffraction signals in the calculated pattern (Figure 9B) are not generated. Again, the overall match of relative intensities is good.

Discussion and Conclusions

The X-ray diffraction evidence supports a cross-β sheet structure for both the Aβ(11–25) and Aβ(1–40) peptide amyloid fibrils. The shorter peptide fragment Aβ(11–25)

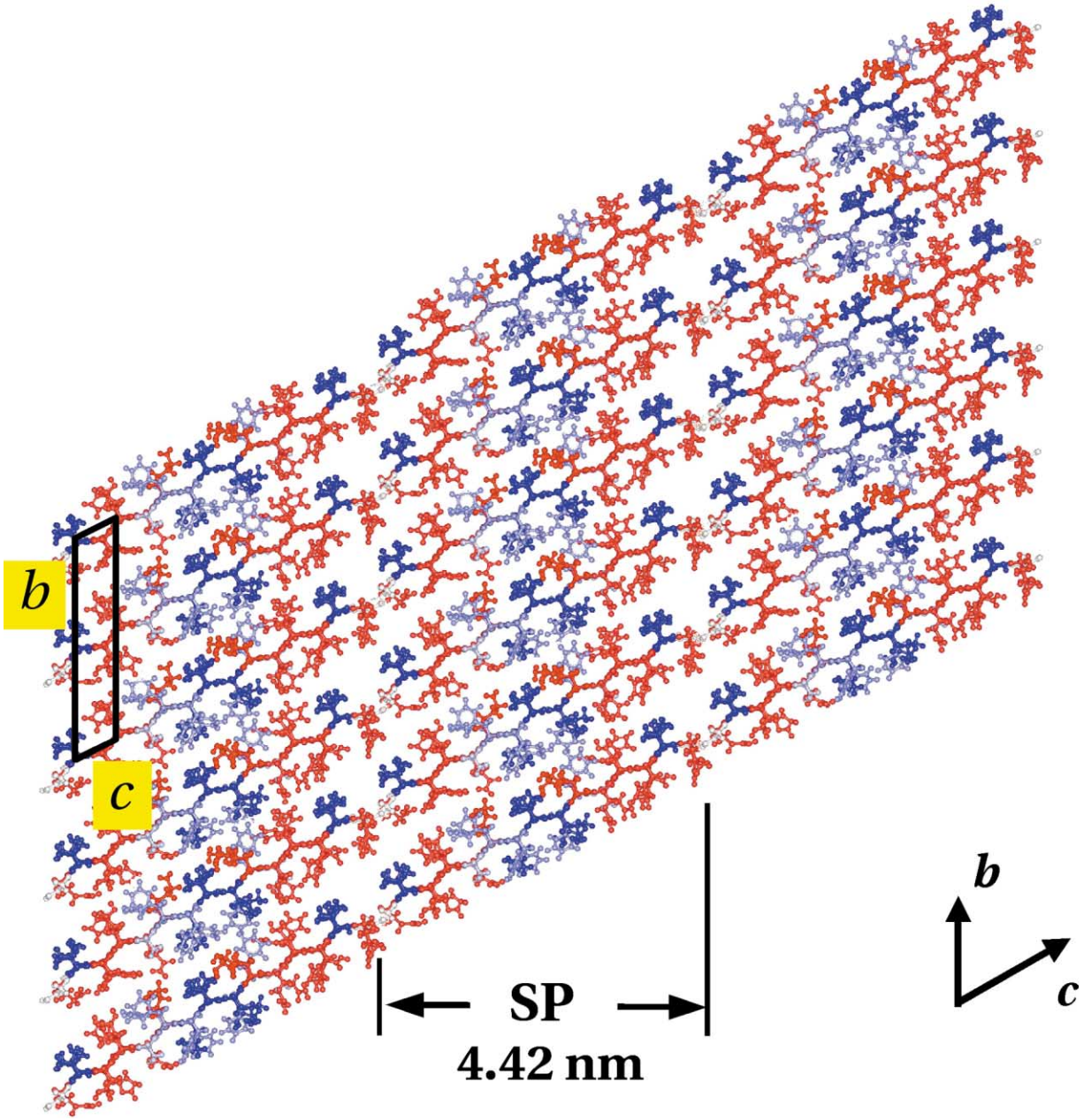

Figure 8. View of the Proposed Structure for Aβ(11–25) Crystals, Viewed Parallel to the *a* Axis (Hydrogen-Bonding Direction)

The wide-angle X-ray diffraction patterns (Figures 2C and 3) emanate from the structure in the monoclinic unit cell (sublattice) shown. The small-angle superlattice diffraction signals (4.42 nm and two orders; Figures 5 and 6A) emanate from the one-dimensional (stacking periodicity; SP) of the cross-β nanotapes that run into the plane of the figure (*a* axis). This lattice is not highly ordered because only three successively attenuating orders of diffraction appear.

is in the central region of the physiologically important longer molecule, and therefore is likely to be involved in the formation of the core structure within Alzheimer's amyloid fibrils (Serpell and Smith, 2000; Serpell et al., 2000). Both these peptides self-assemble via hydrogen bonding (*a*-direction) to form β ribbons. In the case of the 15-mer Aβ(11–25) molecules, the ribbons are composed of antiparallel β sheets in a cross-β arrangement and with the ribbon width the same as the length of the molecule in the β conformation, that is, approximately 5 nm. In the case of the Aβ(1–40) amyloid, the maximum ribbon width (7 nm) seen using transmission electron microscopy is about half that of the molecule in its fully extended β conformation.

Both the wide-angle and small-angle X-ray diffraction data from oriented samples of Aβ(11–25) favor a structure where the cross-β ribbons stack at a distance of 1.06 nm apart to form nanotapes. An intriguing feature of this stacking is that successive ribbons progressively slip by one crimp (0.697 nm) in the *c*-direction, thus

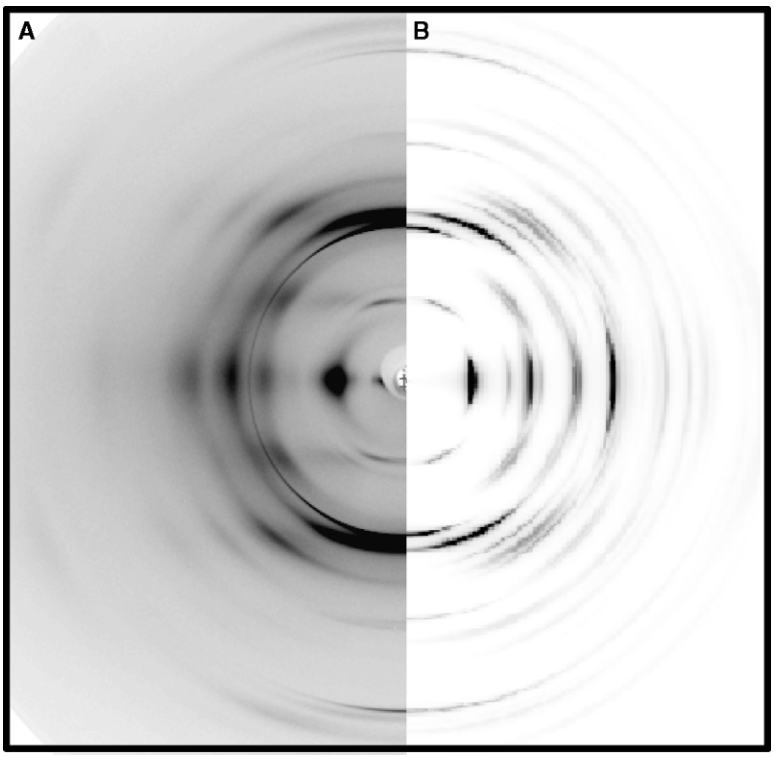

Figure 9. Comparison of the Wide-Angle Experimental X-Ray Diffraction Pattern (Figure 2C) from Aβ(11–25) and the Calculated X-Ray Diffraction Pattern

Experimental (A) and calculated (B) from the proposed model (Figures 7C and 8).

foreshortening the nanotape thickness from 5 nm to 4.42 nm. An explanation for this progressive slip is that if the sheets attempt to stack with zero *c* axis slip, poorer intersheet stacking is possible and consequently the ribbons find a more comfortable stacking arrangement by slipping one *c* axis structural unit. We have not been able to establish any obvious reason for this to occur from examination of the amino acid side chain distribution between adjacent surfaces of Aβ(11–25) ribbons. Unfortunately, calculations based on the spatial arrangement of the side chains are frustrated by the many possible geometric conformations for the various side chains involved. The progressive slip could also arise from competition between surface free energy and internal free energy terms in the nanotapes.

Previously, Kirschner and colleagues (Inouye et al., 1993; Malinchik et al., 1998) have investigated the structure of synthetic Alzheimer's amyloid fibrils using X-ray diffraction and electron microscopy. A gallery of X-ray diffraction patterns from amyloid fibrils aligned in a magnetic field and formed from many different Aβ peptide fragments was presented. A number of these diffraction patterns were analyzed (Inouye et al., 1993) and suggested to arise β crystallites with hexagonal packing (for a review, see Serpell, 2000). However, our data indicate the presence of a preferred texture within the specimen, which suggests that the fibers or crystallites are not cylindrically averaged. Analysis of Aβ(1–40) fibrils using both cross-sectional electron microscopy and fiber X-ray diffraction yielded a model for the fibril consisting of three to five protofilaments (Malinchik et al., 1998), each modeled as a double-walled cylinder. The model does not clarify how the β strands are arranged within the cylinders, although it suggests that they are composed of tilted chains. Our data are consistent with β strands running orthogonal to the fiber axis. Solid-state NMR studies have suggested a parallel, in-register arrangement for the β chains within the Aβ(1–40) amyloid fibrils (Antzukin et al., 2000; Balbach et al., 2002). The measurement of distances between labeled C^{13} amino acids distributed throughout the peptide suggests that amino acids 12–39 are involved in the core, parallel arranged β structure (Antzukin et al., 2000) and suggests that amino acids 1–9 are not involved in the ordered structure. This yields a length of 9.52 nm for the extended β strands. However, our analysis suggests that this is inconsistent with the size of the amyloid fibrils as seen using TEM and we propose that the Aβ(1–40) peptide folds into a hairpin within the amyloid fibrils. Discussion by Balbach et al. (2002) acknowledges the size differences and suggests that a turn or bend may occur within the β strand. Site-directed spin labeling measurements on Aβ(1–40) (Torok et al., 2002) indicate that there may be a turn or bend located between amino acids 23–29, and also support a parallel arrangement for the Aβ(1–40) peptide within the fibrils. It is possible that there could be a mixture of parallel and antiparallel β structure arrangement within the fibrils (Serpell, 2000). However, further investigation is necessary to establish the exact nature of the β strand arrangement. A parallel β sheet arrangement has also been suggested for Aβ(10–35) amyloid fibrils (Benzinger et al., 1998, 2000). In the case of our Aβ(11–25) amyloid fibrils, prepared by both self-assembly and alignment in a magnetic field and by drawing fibers, the cross-β nanotape crystals formed by an antiparallel arrangement of extended β strands.

Here, we present a structure for the arrangement of

Aβ(11–25) molecules within a fibrillar crystal. We have shown that aligned nanotapes stack to form layered crystals with a layer periodicity of 4.42 nm and slippage between the stacked β ribbons provides tight packing of the structure.

Biological Implications

Alzheimer's disease is characterized by the deposition of amyloid fibrils, and the accumulation of amyloid is thought to be central to the disease pathology. The fibrils are formed by ordered aggregation of the Aβ peptide. Knowledge of the structure of the amyloid fibril is essential for understanding how deposition occurs in disease and also the process by which normally soluble proteins undergo conformational change and form insoluble, ordered aggregates. The eventual aim is to be able to rationally design therapeutic molecules to prevent aggregation. Here, we have examined the structure of amyloid fibrils formed from both full-length and a central fragment of Aβ. X-ray diffraction images were collected from aligned synthetic amyloid fibril specimens. The highly oriented nature of the Aβ(11–25) amyloid fibrils has allowed us to present a structure for these fibrous crystals. The crystalline structures in a sample self-assembled and concomitantly oriented in a 2 Tesla magnetic field and prepared by drawing a fiber are the same. However, the oriented texture that develops in a magnetic field provides additional X-ray diffraction data that aid in the structural analysis of the Aβ(11–25) crystals. In these crystals, β ribbons are composed of the 15-mer in an extended β conformation. These ribbons slip relative to one another to form a stable packing arrangement. These results have allowed us to discuss the structure for amyloid fibrils formed from full-length Aβ in disease.

Experimental Procedures

Materials

The 40-mer Aβ(1–40) was purchased from Bachem with the amino acid sequence (H_2N-DAEFRHDSGYEVHHQKLVFFAEDVGSNKGAIIGL MVGGVV-COOH). The 15-mer Aβ(11–25) was synthesized as previously described (Serpell et al., 2000) with the sequence (H_2N-EVHHQKLVFFAEDVG-COOH).

Transmission Electron Microscopy

The lyophilized peptides were dissolved in milliQ-filtered water at a concentration of 10 mg/ml. After incubation of weeks, the solutions were diluted to 1 mg/ml for Aβ(1–40) and to 0.1 mg/ml for Aβ(11–25) for examination by TEM. A 4 μl droplet of each was placed on carbon, pioloform-coated copper grids, blotted, washed, and stained using 2% (w/v) uranyl acetate solution. A Philips 208 transmission electron microscope, operated at 80 kV, was used to study and record images of the Aβ(11–25) and Aβ(1–40) peptide samples.

X-Ray Diffraction

Viscous aqueous solutions (2% w/v) of the Alzheimer's Aβ peptides were gently sucked into a siliconized glass tube of internal diameter 0.7 mm and the oligopeptide molecules were allowed to crystallize until dry (several days) in an orienting magnetic field of magnetic flux density 2 Tesla. For fibers, a drop of the Aβ fragments in the form of a viscous, aqueous solution was placed between the two sides of a stretching frame, as previously described (Serpell et al., 1999) and allowed to dry, resulting in an oriented fiber. X-ray diffraction patterns were taken at the European Synchrotron Research Facility (ESRF) in Grenoble, France using a wavelength of 0.09515 nm and recorded on a MAR research image plate detector (300 mm diameter) as previously described (Serpell et al., 2000). The specimen was initially mounted with the major alignment axis normal to the incident beam and near zero tilt. This was achieved by rotating the sample until the intensities of the diffraction signals above and below the equator were symmetrical. Additional patterns were collected using a rotating anode and wavelength 0.15418 nm (Cu Kα), equipped with a MAR research image plate (diameter 180 mm). X-ray diffraction patterns were recorded at rotations of 90°, parallel to the axis of the alignment axis and at right angles to the initial direction. A low-angle pattern was recorded on photographic film, with a specimen to film distance of 289.4 mm using a rotating anode Cu Kα source.

Modeling

The software packages Cerius2 and InsightII (MSI) were used in structural modeling and diffraction simulations. Care was taken to ensure that the models were stereochemically sound and that the simulated diffraction patterns were in good agreement with the experimental data. In the computer-simulated X-ray diffraction patterns, the temperature factor and degree of arcing were chosen to match the experimental X-ray diffraction pattern as closely as possible.

Acknowledgments

We wish to thank Dr. B. Rasmussen and colleagues at ESRF, Grenoble and Dr. J. Harford, Imperial College, London University for their valuable assistance in the collection of the X-ray data. We thank the Engineering and Physical Sciences Research Council for supporting this work, a including postdoctoral fellowship to P.S. L.C.S. is supported by a Wellcome Trust RCDF. L.C.S. wishes to acknowledge her affiliation with the Neurobiology Division, MRC Laboratory of Molecular Biology, Cambridge, UK.

Received: October 1, 2002
Revised: May 19, 2003
Accepted: May 21, 2003
Published: August 5, 2003

References

Alexander, L.E. (1969). X-Ray Diffraction Methods in Polymer Science (New York: Wiley Interscience).

Antzukin, O.N., Balbach, J.J., Leapman, R.D., Rizzo, N.W., Reed, J., and Tycko, R. (2000). Multiple quantum solid-state NMR indicates a parallel, not antiparallel organization of β-sheets in Alzheimer's β-amyloid fibrils. Proc. Natl. Acad. Sci. USA *97*, 13045–13050.

Balbach, J.J., Petkova, A.T., Oyler, N.A., Antzukin, O.N., Gordon, D.J., Meredith, S.C., and Tycko, R. (2002). Supramolecular structure in full-length Alzheimer's β-amyloid fibrils: evidence for parallel β-sheet organization from solid state nuclear magnetic resonance. Biophys. J. *83*, 1205–1216.

Benzinger, T.L.S., Gregory, D.M., Burkoth, T.S., Miller-Auer, H., Lynn, D.G., Botto, R.E., and Meredith, S.C. (1998). Propagating structure of Alzheimer's β-amyloid (10–35) is parallel β-sheet with residues in exact register. Proc. Natl. Acad. Sci. USA *95*, 13407–13412.

Benzinger, T.L.S., Gregory, D.M., Burkoth, T.S., Miller-Auer, H., Lynn, D.G., Botto, R.E., and Meredith, S.C. (2000). Two-dimensional structure of β-amyloid(10–35) fibrils. Biochemistry *39*, 3491–3499.

Eanes, E.D., and Glenner, G.G. (1968). X-ray diffraction studies on amyloid filaments. J. Histochem. Cytochem. *16*, 673–677.

Fraser, R.D.B., and MacRae, T.P. (1973). Conformation in Fibrous Proteins and Related Synthetic Polypeptides (New York: Academic Press).

Geddes, A.J., Parker, K.D., Atkins, E.D.T., and Beighton, E. (1968). "Cross β" conformation in proteins. J. Mol. Biol. *32*, 343–358.

Inouye, H., and Kirschner, D.A. (1997). X-ray diffraction analysis of scrapie prion: intermediate and folded structures in a peptide containing two putative α-helices. J. Mol. Biol. *268*, 375–389.

Inouye, H., Fraser, P.E., and Kirschner, D.A. (1993). Structure of

β-crystallite assemblies by Alzheimer β amyloid protein analogues: analysis by X-ray diffraction. Biophys. J. *64*, 502–519.

Keith, H.D., Giannoni, G., and Padden, F.J. (1969). Single crystals of poly-L-glutamic acid. Biopolymers *7*, 775–792.

Krejchi, M.T., Cooper, S.J., Deguchi, Y., Atkins, E.D.T., Fournier, M.J., Mason, T.L., and Tirrell, D.A. (1997). Crystal structures of chain-folded antiparallel β-sheet assemblies from sequence-designed periodic polypeptides. Macromolecules *17*, 5012–5024.

Malinchik, S.B., Inouye, H., Szumowski, K.E., and Kirschner, D.A. (1998). Structural analysis of Alzheimer's β(1–40) amyloid: protofilament assembly of tubular fibrils. Biophys. J. *74*, 537–545.

Naiki, H., Higuchi, K., Hosokawa, K., and Takeda, T. (1989). Fluorometric determination of amyloid in vitro using the fluorescent dye, thioflavine T. Anal. Biochem. *177*, 244–249.

Pauling, L., and Corey, R.B. (1953). Two β-pleated sheet configurations of polypeptide chains involving both cis- and trans-amide groups. Proc. Natl. Acad. Sci. USA *39*, 253–256.

Puchtler, H., Sweat, F., and Levine, M. (1961). On the binding of Congo red by amyloid. J. Histochem. Cytochem. *10*, 355–364.

Rudall, K.M. (1946). The structure of epidermal protein. In Symposium on Fibrous Proteins, University of Leeds, J. Soc. Dyers and Colourists, pp. 15–23.

Rudall, K.M. (1950). Fundamental structures in biological systems. In Progress in Biophysics and Biophysical Chemistry, Volume 1, J.A.V. Butler and J.T. Randall, eds. (London: Butterworth-Springer), pp. 39–72.

Rudall, K.M. (1952). The proteins of the mammalian epidermis. In Advances in Protein Chemistry, Volume VII, M.L. Anson, K. Bailey, and J.T. Edsall, eds. (New York: Academic Press), pp. 253–290.

Selkoe, D.J. (1991). The molecular pathology of Alzheimer's disease. Neuron *6*, 487–498.

Serpell, L.C. (2000). Alzheimer's amyloid fibrils: structure and assembly. Biochim. Biophys. Acta *1502*, 16–30.

Serpell, L.C., and Smith, J.M. (2000). Direct visualisation of the β-sheet structure of Alzheimer's amyloid. J. Mol. Biol. *299*, 225–231.

Serpell, L.C., Fraser, P.E., and Sunde, M. (1999). X-ray fiber diffraction of amyloid fibrils. Methods Enzymol. *309*, 526–536.

Serpell, L.C., Blake, C.C.F., and Fraser, P.E. (2000). Molecular structure of a fibrillar Alzheimer's Aβ fragment. Biochemistry *39*, 13269–13275.

Sunde, M., and Blake, C.C.F. (1998). From the globular to the fibrous state: protein structure and structural conversion in amyloid formation. Q. Rev. Biophys. *31*, 1–39.

Sunde, M., Serpell, L.C., Bartlam, M., Fraser, P.E., Pepys, M.B., and Blake, C.C.F. (1997). Common core structure of amyloid fibrils by synchrotron X-ray diffraction. J. Mol. Biol. *273*, 729–739.

Torok, M., Milton, S., Kayed, R., Wu, P., McIntire, T., Glabe, C.G., and Langen, R. (2002). Structural and dynamic features of Alzheimer's Aβ peptide in amyloid fibrils studied by site-directed spin labeling. J. Biol. Chem. *277*, 40810–40815.

Virchow, R. (1854). Zur Cellulose-Frage. Virchows Arch. *6*, 415–426.

Worcester, D.L. (1978). Structural origins of diamagnetic anisotropy in proteins. Proc. Natl. Acad. Sci. USA *75*, 5475–5477.